Results in Control and Optimization 22 (2026) 100661

Contents lists available at ScienceDirect

Results in Control and Optimization

journal homepage: www.elsevier.com/locate/rico

Analysis of the efficacy of the risk-based $\bar{X}$ control chart in statistical process control

Aamir Saghir [a], Attila I. Katona [b], Csaba Hegedũs [c], Zsolt T. Kosztyán [b,d,*]

[a] Department of Statistics, Mirpur University of Science and Technology (MUST), Mirpur, 10250, AJK, Pakistan
[b] Department of Quantitative Methods, University of Pannonia, Egyetem str.10, Veszprem, 8200, Hungary
[c] Department of Supply Chain Management, University of Pannonia, Egyetem str.10, Veszprem, 8200, Hungary
[d] Institute of Advanced Studies, Koszeg (iASK), Charnel str. 14, Koszeg, 9730, Hungary

ARTICLE INFO

Keywords:
Average run length
Control charts
Optimization
Phases I and II
Process shift
Risk-based methodology
Statistical process control

ABSTRACT

Risk-based control charts have recently been introduced to address measurement uncertainty. The statistical properties of a risk-based control chart for detecting a shift have not been studied. In addition to the control chart design, performance evaluation is important for detecting changes in the process. In this paper, the effectiveness of a risk-based $\bar{X}$ control chart (recently introduced) in the presence of measurement uncertainty is investigated. By utilizing a risk-based model that considers the cost of decision outcomes, the impact of measurement uncertainty on the $\bar{X}$ chart's performance in both in- and out-of-control scenarios is designed and examined. To lessen the risk associated with measurement uncertainty, the Nelder–Mead search technique is employed to find the optimal control limits. The performance metrics include the total decision cost, cost ratio, probability ratio, and average run length. Simulation and real-world data analyses are employed to assess the efficiency of the risk-based chart via various performance metrics. A sensitivity analysis is conducted to identify the constraints and relevance of the risk-based $\bar{X}$ chart in statistical process control.

1. Introduction

Statistical process control (SPC) is a technique that is typically employed in operations management to regulate a process or production method. Control charts are a key tool of SPC employed to assess whether a company or manufacturing process is in a condition of control, meaning that it is stable and varies only from sources common to the process. [1]. In SPC, a process is considered statistically controlled when the measured values of a product attribute stay within the specified limits [2]. A control chart is designed to monitor process stability and identify assignable causes quickly. The design of the control chart involves information about the statistical distribution of quality characteristics, sample size (n), sampling interval (h), plotting statistics, and control limits (lower, center, and upper limits) [1,3,4]. Typically, these parameters are chosen on the basis of only statistical criteria, including the average count of samples collected before a signal is triggered, known as the average run length (ARL). The effectiveness of the control chart is gauged by the speed at which a change in the process parameter is identified; this can be articulated in terms of the ARL. Consequently, the selection of the statistical restriction depends on the control chart's configuration, which should exhibit a high in-control ARL value before signaling when the process remains under control and a low out-of-control ARL value upon any change in one or more process parameters. Therefore, a control chart's efficacy and performance evaluation are crucial in addition to design.

* Corresponding author at: Department of Quantitative Methods, University of Pannonia, Egyetem str.10, Veszprem, 8200, Hungary.
E-mail address: kosztyan.zsolt@gtk.uni-pannon.hu (Z.T. Kosztyán).

https://doi.org/10.1016/j.rico.2026.100661
Received 20 July 2025; Received in revised form 27 November 2025; Accepted 22 January 2026
Available online 23 January 2026
2666-7207/© 2026 The Authors. Published by Elsevier B.V. This is an open access article under the CC BY license (http://creativecommons.org/licenses/by/4.0/).

The $\bar{X}$ control chart, introduced by Shewhart [2], is utilized by many companies to enhance process quality. A key benefit is its straightforward setup and ease of use, leading to its widespread application in controlling the variability in the quality attribute of concern for a product or service [5]. Nonetheless, it is somewhat less responsive to minor and moderate alterations and considers independent and identically distributed (iid) data points. When data are autocorrelated or nonnormally distributed, the control chart's efficacy decreases because if not accounted for during design, this data behavior increases the probability of false alarms [6–8]. Moreover, economic aspects are not specifically considered in the statistical construction of the $\bar{X}$ control chart. Because of this, Duncan [9] presented the economic design of the Shewhart chart, in which the predicted cost function is minimized to establish the parameters. Various authors have created distinct modifications (economic and adaptive) of the classic $\bar{X}$ chart to increase its effectiveness in identifying small and moderate shifts [10–13].

Nonnormality and independence are not the only factors that can reduce the effectiveness of the traditional $\bar{X}$ chart. The chart functions on a reliability foundation and neglects the measurement uncertainty (MU) [14–17]. Nonetheless, the MU of the system results in faulty choices such as unwarranted production halts or overlooked actions [18,19], and the impact of measurement uncertainty on statistical process control has been studied by Abraham [20]; Asif et al. [21]; Hu et al. [22]; Linna et al. [23]; Maravelakis [24]; Sabahno et al. [25]; Saghaei et al. [26]; Aslam [27]; Zaidi et al. [28]; Jawad Mirza et al. [29]; Carrillo et al. [30]; Shojaee et al. [31]; Ahmadini et al. [32] and references therein. Consequently, the creation of innovative approaches to reduce the number of erroneous decisions during the assessment of effects is crucial for SPC research and requires investigation.

In the literature, numerous approaches have been proposed to optimize the cost or risk arising because of the measurement uncertainty of the system (see [31,33]). All these approaches are based on either statistical design (SD), economic design (ED) or economic statistical design (ESD) to optimize the process cost or risk adjustment. However, no approach considers the cost of the decision of outcomes of the process in designing the control chart and overall adjusting the risk together. A risk-based (RB) strategy was developed as a solution by Kosztyán et al. [34] that considers all possible outcomes to minimize the chances of erroneous results amid parameter uncertainty. The risk-based control charts use simulation and optimization to select the optimal values of the chart parameters to minimize the risks arising from incorrect decisions related to process control. In contrast to Shewhart and ESD control charts, the RB strategy considers the effect of measurement errors and accounts for the costs of each decision outcome during control chart design [34]. Despite the nonnormal distribution of measurement errors, the risk-based strategy was highly successful in lowering decision costs. Subsequently, Hegedűs and Kosztyán [35]; Kosztyán et al. [36] examined a risk-based method in conformity testing, whereas Hegedűs et al. [37]; Kosztyán and Katona [38]; Kosztyán and Katona [39] created risk-based control charts for managing statistical processes. Katona [16] confirmed the potency of the risk-based approach in compliance and control charts by using industrial datasets. Katona et al. [40] developed univariate risk-based charts on average by considering measurement uncertainty. Saghir et al. [41] designed two new RB average control charts for monitoring the autoregressive processes. The results from all these studies show that a risk-based approach effectively reduces decision costs. However, all these investigations focused solely on risk-based control charts, and there has been no research assessing the statistical effectiveness of these charts in identifying a shift (assignable cause) in the process within the literature. This represents a significant research void in the SPC literature, and this study seeks to address it.

The primary objectives of this study are to (i) investigate and assess the statistical effectiveness of the univariate risk-based $\bar{X}$ chart amid measurement uncertainty, (ii) analyze the statistical indicators both in situations that are within control and those that are not, (iii) confirm the findings through simulation and actual data, and (iv) offer practical advice to engineers and decision makers. This is how the rest of the article is organized: Section 2 outlines the risk-oriented structure of the $\bar{X}$ chart. The performance metrics of the risk-based $\bar{X}$ are established in Section 3 for both in-control and out-of-control process conditions. The findings are shown in Section 4. A sensitivity analysis is given in Section 5. Section 6 concludes the article with a summary and suggestions for the future.

2. The risk-based design of the $\bar{X}$ chart

According to Kosztyán and Katona [39], the risk-based $\bar{X}$ control chart can be developed for Phase-I analysis in the following four steps: (1) determining the parameters for the traditional control chart, (2) assessing decision costs, (3) calculating total costs, and (4) optimizing the control limit.

2.1. Calculation of limits

Let X_{ij} be an ith ($i = 1, 2, \ldots, m$) sample of size j ($j = 1, 2, \ldots, n$) drawn i.i.d. from any parent distribution having $E(X) = \mu$ and variance $(X) = \sigma^2$. For simplicity, we assume that $X_{i,j} \sim N(\mu, \sigma^2)$. The sample statistics for the ith sample for the $\bar{X}$ chart can be computed as follows [42]:

$$\bar{X}_i = \frac{1}{n}\sum_{j=1}^{n} X_{ij}, \quad i = 1, 2, \ldots, m \tag{1}$$

The sampling distribution of $\bar{X}_i \sim N(\mu, \sigma^2/n), \forall i = 1, 2, \ldots, m$ [1]. The control limits of the $\bar{X}$ chart can be calculated as follows:

$$UCL_{\bar{X}} = \mu + k_u \frac{\sigma}{\sqrt{n}} \tag{2}$$

$$LCL_{\bar{X}} = \mu - k_l \frac{\sigma}{\sqrt{n}} \tag{3}$$

Table 1
Results of a statistical process control decision.

Actual feature property	Noticed feature property	
	In-control	Out-control
In-control	c_{11}	c_{10}
Out-control	c_{01}	c_{00}

where μ denotes the average and σ denotes the standard deviation of the data; k_l and k_u are the lower and upper quantile points, respectively, of the sampling distribution of the means for a prespecified false alarm rate, usually set α=0.0027 [1]; and $UCL_{\bar{X}}$ and $LCL_{\bar{X}}$ denote the upper and lower control limits, respectively. In the case of a symmetric (like normal) distribution, $k_l = k_u = k$. The process parameters in applications are typically unknown and are calculated via preliminary samples (Phase I) under the assumption of an in-control process. On the basis of these data, the average μ is calculated as follows:

$$\bar{\bar{X}} = \frac{1}{m}\sum_{i=1}^{m}\bar{X}_i = \frac{1}{m}\sum_{i=1}^{m}\left(\frac{1}{n}\sum_{j=1}^{n}X_{ij}\right) \tag{4}$$

and the process standard deviation σ is determined from the standard deviation of the sample mean $\bar{X}_i$ as follows:

$$s = \left(\frac{1}{m-1}\sum_{i=1}^{m}(\bar{X}_i - \bar{\bar{X}})^2\right)^{\frac{1}{2}} \tag{5}$$

The sample estimate of the standard deviation defined in Eq. (5) is a biased estimator of σ. In the SPC literature, it is recommended to adjust s for unbiasedness via s/c_4, where c_4 is an unbiased constant that depends on sample size (n) and is tabulated in [1] and other related books.

2.2. Cost estimation

Measurement uncertainty can be determined via measurement error models: (i) a simple additive model and (ii) a linear covariate measurement model. Bennett [43] were the pioneers who investigated the effect of measurement errors on the $\bar{X}$ chart using a simple additive model. Later, Abraham [20]; Kanazuka [44]; Mittag and Stemann [45]; Kosztyán et al. [36] used this simple additive model in control charts and acceptance sampling. Linna and Woodall [46] introduced a more general linear covariate error model, which has been considered in many studies, including [25,28,30], etc. In this work, we have considered the simple additive model proposed by Bennett [43] because it is a simple and fundamental model in error modeling. Moreover, the conformity of the product is judged on the basis of the observed (measured) value following Kosztyán et al. [34]; Kosztyán and Katona [39]. However, further study may be conducted using a linear covariate error model in RB control charts.

Owing to measurement errors (ϵ) distorting the true value of the monitored product characteristic (x), each observed value (y) can be represented by the simple linear model in the following way:

$$y_i = x_i + \epsilon_i, i = 1, 2, \ldots, m. \tag{6}$$

where x refers to the measured product characteristic without the MU, ϵ is the measurement uncertainty/error of the system (independent of x) and y represents the observed values that contain the MU. The probability density functions (PDFs) of x and ϵ are presumed to be known. Moreover, the PDF of ϵ can be obtained from the producer's documentation on the measuring instrument and the analysis of the measurement system, or it can be approximated from the calibrations. For simplicity, we assume that $\epsilon_{i,j} \sim N(0, \sigma_\epsilon^2)$; however, any parent distribution can be assumed to have an expected value of 0.

On the basis of the real characteristics (x) and observed values with the MU (y) of an SPC, the results of the $\bar{X}$ chart can be categorized as follows: (i) correct acceptance, (ii) type I error, (iii) type II error, and (iv) correct control. Table 1 illustrates the arrangement of the decision cost results on the basis of the actual and observed characteristics of the product.

where c_{11} represents the cost of correct acceptance, c_{10} is the cost of a type I error (false control), c_{01} signifies the cost of a type II error (false acceptance), and c_{00} refers to the cost of correct control when an out-of-control condition is accurately identified.

By examining the cost components obtained from the manufacturer's ERP system, the cost of each choice can be assessed. For a more thorough explanation of decision cost estimation, readers are encouraged to consult [38], which outlines the key components and offers a practical example of the estimation procedure.

2.3. Calculation of total cost

ED control charts, proposed by Duncan [9], involve determining key chart parameters (such as sample size, control limits, and sampling intervals) to achieve minimum expected cost (operational costs). In contrast, the RB approach emphasizes the consequences of decision-making (measured in terms of cost) rather than the operational costs of the control process itself. It focuses on the cost of wrong decisions, such as failing to detect an out-of-control condition or issuing a false alarm during process monitoring. Therefore, a new evaluation measure, namely, total decision cost (TC), was formulated by Kosztyán and Katona [38], which determined the total

cost while considering all the consequences during process monitoring. Mathematically, the TC (an economic measure) considering the decision outcomes and associated cost of each decision given in Table 1 is defined as follows:

$$TC = C_{11} + C_{10} + C_{01} + C_{00} = q_{11}c_{11} + q_{10}c_{10} + q_{01}c_{01} + q_{00}c_{00} \tag{7}$$

where C_{ab} represents the total cost associated with a particular decision outcome, q_{ab} indicates the number of instances (cases) that occurred during the control and c_{ab} denotes the cost of each decision estimated/assessed by the ERP system (see [40]).

2.4. Optimization

In applications, the actual quality features $X_{i,j}$ are not immediately visible; instead, they can be evaluated only on the basis of the outcomes $(Y_{1,j}, Y_{2,j}, \ldots, Y_{m,j})$ of a collection of $m \geq 1$ measurement procedures, each of which equals the simple linear error model defined in Eq. (6). For sample ith, the sample statistics for $\bar{X}$ based on observable measurements $Y_{i,j}$ with the MU can be computed as follows:

$$\bar{Y}_i = \frac{1}{n}\sum_{j=1}^{n} Y_{ij} = \frac{1}{n}\left(\sum_{j=1}^{n} X_{ij} + \sum_{j=1}^{n} \epsilon_{ij}\right) = \bar{X}_i + \bar{\epsilon}_i, \quad i = 1, 2, \ldots, m \tag{8}$$

The sampling distribution of $\bar{Y}_i \sim N\left(\mu, \frac{\sigma^2+\sigma_\epsilon^2}{n}\right)$ is because $E(\epsilon_i) = 0$, where σ_ϵ^2 is assumed to be a constant and is independent of the process mean μ.

Thus, the control limits of the risk-based $\bar{X}$ chart under the MU are defined as follows:

$$UCL_{\bar{X}_{rb}} = \mu + k_x \frac{(\sigma + \sigma_\epsilon)}{\sqrt{n}} \tag{9}$$

$$LCL_{\bar{X}_{rb}} = \mu - k_x \frac{(\sigma + \sigma_\epsilon)}{\sqrt{n}} \tag{10}$$

where k_x is a charting parameter of the risk-based mean chart and is chosen to minimize the expected losses or risks by decision outcomes, not simply set at a quantile for a fixed type I error rate (α), as is typically done in risk-adjusted control charts. Unlike risk-adjusted charts [47], which account for measurement error but do not incorporate the costs or impacts of decisions, the risk-based approach explicitly integrates these considerations into the chart design.

To find the optimal limits for the risk-based $\bar{X}$ chart, the total decision cost (TC) is reduced by fine-tuning the charting parameters k_x in the following manner:

$$\begin{aligned} &\underset{(k_x)}{\text{minimize}} \quad TC(k_x) \\ &\text{subject to} \quad k_x > 0 \\ &\qquad\qquad \forall \quad k_x \in \mathbf{R} \end{aligned} \tag{11}$$

Eq. (11) is a simple optimization problem and can be solved via any optimization method, such as the Nelder–Mead approach or the genetic algorithm. Let k_x^* be an optimal solution of Eq. (11), which denotes the optimal correction constant depending on the sample size (n), the observed process distribution, the measurement error distribution, and the decision outcome costs (c_{ab}). It minimizes the total loss from these choices while striking a balance between type I and type II errors. This approach allows greater flexibility and realism, especially in contexts where the costs of false alarms and missed detections are asymmetric or context dependent.

3. Performance measures

The efficiency of a control chart is typically assessed by its ARL, defined as the anticipated count of observations presented on a control chart before an alert is activated [1]. Until a process operates at an in-control state, the ARL (denoted by ARL_0) is desired to be sufficiently large, usually $ARL_0 = 370.4$, because an alarm would be a misleading indication. Conversely, an alert from the control chart for a process that is out of control, i.e., a genuine signal, must be generated as soon as possible so that the ARL (represented by ARL_1) reflecting the detection delay remains minimal. Readers are referred to [1,48] for detailed information on how to measure the efficiency of control charts. In SPC, a control chart (CC) is assessed using either a zero-state (ZS) or a steady-state (SS) ARL. The SSARL measures the average time required for the CC to identify a process shift for control statistics to reach a static distribution. While ZSARL is the number of samples taken from the start of signal monitoring in an out-of-control situation (cf., [49,50]). In this study, we use ZSARL to compare the performance of the charts under study.

If the process deviates from the standard specifications, it should be identified as feasible, considering the modifications (shifts) in terms of standard deviation units, i.e., $\mu_1 = \mu_0 + \delta\sigma_0$, $\delta \in R$. In terms of statistical inference, the performance of a CC is equivalent to testing the hypotheses;

$$H_0 : \mu_1 = \mu_0 \quad \text{vs} \quad H_a : \mu_1 \neq \mu_0$$

The process is operating in a control state when $\delta = 0$, and the average does not change ($\mu_1 = \mu_0$). In contrast, when $\delta > 0$ or $\delta < 0$, the average shifts upward (positive) or downward (negative), and the process moves into an out-of-control state ($\mu_1 \neq \mu_0$).

The risk-based $\bar{X}$ chart is designed on the basis of all four decision outcomes of a process as described in Section 2. Stated differently, it is designed on the basis of the joint distribution of x and y, characteristics with all possibilities. The evaluation of the risk-based $\bar{X}$ chart in a given state, either $\delta = 0$ or $\delta \neq 0$, is determined through conditional analysis (performance) of these limits under the given condition, i.e., the evaluation of y's conditional distribution given x. If H_0 is true, the decision outcomes of the process under **in-control** conditions (i.e., $\delta = 0$) correspond to the cases in the first row of Table 1. The total conditional cost of the process under H_0 is then calculated as follows:

$$TC_{In} = C_{11} + C_{10} = q_{11}c_{11} + q_{10}c_{10} \tag{12}$$

where C_{ab}, q_{ab} and c_{ab} have the same meaning as defined in Eq. (7).

Thus, the probability of type I error (α) of the risk-based $\bar{X}$ chart is as follows:

$$\begin{aligned}\alpha &= Prob(\text{conditional decision outcome } q_{10})\\ &= Pr\left(\bar{y} \notin \left(LCL_{rb}, UCL_{rb}\right) \text{ and } \bar{x} \in (LCL, UCL) \mid \ \delta = 0\right)\\ &= Pr\left(\bar{y} \notin \left(LCL_{rb}, UCL_{rb}\right) \mid \bar{x} \in (LCL, UCL), \delta = 0\right).Pr\left(\bar{x} \in (LCL, UCL) \mid \delta = 0\right)\\ &= \int_{\bar{y} \notin (LCL_{rb}, UCL_{rb})} f_{\bar{y}}(\bar{y} \mid \bar{x} \in (LCL, UCL))\, d\bar{y}. \int_{\bar{x} \in (LCL, UCL)} f(\bar{x})\, d\bar{x}\end{aligned}$$

where $f_{\bar{y}}(\bar{y}|\bar{x} \in (LCL, UCL))$ is the probability density function of the observed mean given the actual process state. The joint distribution of ($\bar{y}$, $\bar{x}$) and/or the conditional distribution of ($\bar{y}|\bar{x}$) are required to evaluate the above integral under H_0. When x_i is normally distributed and y_i is a linear model, as assumed in our study, then the joint distribution of $\bar{x}_i$ and $\bar{y}_i$ is a bivariate normal distribution, i.e., $\left(\bar{x}_i, \bar{y}_i\right) \sim BVN\left(\begin{pmatrix}\mu\\ \mu\end{pmatrix}, \begin{pmatrix}\sigma^2 & \sigma^2\\ \sigma^2 & \sigma^2 + \sigma_c^2\end{pmatrix}\right)$. Analytically, evaluating this integral is more complicated. Alternatively, simulation studies can be used to evaluate α by the conditional count of q_{10} based on the samples numerically. It can be defined as follows:

$$\alpha = \frac{n\left(\bar{y} \notin \left(LCL_{rb}, UCL_{rb}\right) \cap \bar{x} \in (LCL, UCL) \mid \delta = 0\right)}{n(S)} \tag{13}$$

where $n(A)$ denotes the number of favorable outcomes and $n(S)$ denotes the total number of outcomes in the simulation. Similarly, the decision outcomes correspond to the cases in the second row of Table 1 when a shift occurs ($\delta \neq 0$). Moreover, the total conditional decision cost of the process for the **out-of-control** state is as follows:

$$TC_{out} = C_{01} + C_{00} = q_{01}c_{01} + q_{00}c_{00} \tag{14}$$

Afterward, the probability of correctly rejecting (1-β) the risk-based $\bar{X}$ chart can be calculated as follows:

$$\begin{aligned}1 - \beta &= Prob(\text{conditional decision outcome } q_{00})\\ &= Pr\left(\bar{y} \notin \left(LCL_{rb}, UCL_{rb}\right) \text{and} \bar{x} \notin (LCL, UCL), \delta \neq 0\right).Pr\left(\bar{x} \notin (LCL, UCL) \mid \delta = 0\right)\\ &= \int_{\bar{y} \notin (LCL_{rb}, UCL_{rb})} f_{\bar{y}}(\bar{y} \mid \bar{x} \notin (LCL, UCL))\, d\bar{y}. \int_{\bar{x} \notin (LCL, UCL)} f(\bar{x})\, d\bar{x}\end{aligned}$$

The joint distribution of $\bar{x}$ and $\bar{y}$ or the conditional distribution of $\bar{y}$ given $\bar{x}$ and $\delta \neq 0$ becomes more complex under H_a. Again, simulation can be used to approximate the probability of correctly signaling an out-of-control state as follows:

$$1 - \beta = \frac{n\left(\bar{y} \notin \left(LCL_{rb}, UCL_{rb}\right) \cap \ \bar{x} \notin (LCL, UCL) \mid \ \delta \neq 0\right)}{n(S)} \tag{15}$$

where the conditional count of q_{00} can be obtained from Eq. (14). The total probability of rejecting (signal) the process can be calculated as follows:

$$P(\text{signal}) = p^* = \alpha.P(IC) + (1 - \beta).P(OOC) \tag{16}$$

where $P(IC)$ and $P(OOC)$ are the probabilities of the actual process state being in control and out of control, respectively.

The ARLs of the risk-based $\bar{X}$ chart for both scenarios are computed as follows:

$$ARL_0 = \frac{1}{\alpha} \tag{17}$$

$$ARL_1 = \frac{1}{1 - \beta} \tag{18}$$

Moreover, there is a limit on the overall cost of the risk-based $\bar{X}$ chart design, which is determined by taking the related costs of the four possible outcomes. Therefore, two other performance measures, namely, (i) the cost ratio (CR) and (ii) the probability ratio (PR), (the ratio of the chance of incorrect acceptance/rejection to the chance of correct acceptance/correct rejection), of the associated decision are used for deeper evaluations of the risk-based methodology. These performance measures, when $\delta = 0$ and $\delta \neq 0$, are defined as follows:

$$CR_0 = \frac{C_{10}}{C_{11}} \tag{19}$$

$$PR_0 = \frac{q_{10}}{q_{11}} \tag{20}$$

and

$$CR_1 = \frac{C_{01}}{C_{00}} \tag{21}$$

$$PR_1 = \frac{q_{01}}{q_{00}} \tag{22}$$

, respectively.

4. Numerical results

This section assesses the effectiveness of the risk-based $\bar{X}$ chart in overseeing the process mean amid measurement uncertainty with $\delta = 0$ and $\delta \neq 0$ conditions. First, the simulation outcomes are shown to assess the effectiveness of the risk-based $\bar{X}$ chart for both conditions in Section 4.1. Furthermore, real-world data are utilized to assess the effectiveness of the chart mentioned in Section 4.2.

4.1. Evaluation through simulation

In this subsection, the risk-based $\bar{X}$ is constructed following the methodology of Kosztyán and Katona [38] and Katona et al. [40] for simulated data. The optimized constant for the given chart is found via Eq. (11) through the Nelder–Mead simplex technique. Afterward, the performance metrics of the risk-based $\bar{X}$ chart are examined. All calculations are performed via R software.

Phase I analysis

In the SPC, phase I analysis is conducted to analyze historical data and establish a stable process. It helps in estimating the control limits and detecting special causes to clean the data and achieve a stable, "in-control" process [4]. The simulation is conducted following the work of Katona [16] to design and construct the efficacy of the risk-based $\bar{X}$ chart. We use Phase I samples for both actual and measurement error characteristics drawn from a normal distribution with specified known parameters. Using these samples, the plotting statistics, the average and the standard deviations of the plotting statistics, the charting constant and the control limits are determined without and with optimization. The following steps are executed in the simulation to construct the risk-based $\bar{X}$ chart:

1. Draw a size n random sample drawn from the actual product's distribution (x) and measurement uncertainty (ϵ).
2. Estimate the observed product (y_i) via Eq. (6) from the data generated in step (1).
3. Calculate the sample statistics and control limits for x and y via Eqs. (1)–(10).
4. Determine the number of decisions associated with the statistic via Table 1.
5. Compute the overall decision cost according to Eq. (7).
6. Find the optimal constant via Eq. (11) and modify the control limits.
7. Repeat steps (1–6) 1000 times. At this point, we have the control limits and optimal parameters based on 1000*n observations.
8. Steps (1–7) are iterated 100 times to report the average results.

Algorithm 1 provides a detailed description of the procedure for calculating the optimal chart constant, assessing the total cost, and deriving decision outcomes for the RB chart in Phase I analysis.

Algorithm 1 Pseudocode for the RB chart in Phase I cost optimization

Input: obs, n, μ_X, va_X, sk_X, ku_X, μ_e, va_e, C, confidence_level, bounds $[LKL, UKL]$
Generate true process data $X \leftarrow$ `generate(obs, `μ_X`, `va_X`, `sk_X`, `ku_X`)`
Generate measurement error data $UC \leftarrow$ `data_gen(obs, `μ_e`, `va_e`, 0, 3)`
Define a cost function $f(K) \leftarrow$ total cost from `rbxcc(X, UC, C, n, confidence_level, K)`
Optimize K^* by minimizing $f(K)$ over $[LKL, UKL]$ using numerical optimization
Evaluate the risk-based chart result $H \leftarrow$ `rbxcc(X, UC, C, n, confidence_level, `K^*`)`
Add the optimal K^* to the result: $H.par \leftarrow K^*$
Output: Optimal K^*, total cost (C_0), decision outcomes (P_1 to P_4), control limits (T_1 to T_4), $xbar$, $ybar$

The calculation of the performance of the RB chart in out-of-control scenarios based on the total decision cost, cost ratio, probability of the signal, and average run length is explained in Algorithm 2.

The parameters of the actual process and measurement error distributions, sample size, decision cost and number of repetitions are required inputs of this simulation study. A comprehensive list of the simulation's input parameters, akin to [40], is presented here in Table 2. An actual R code is provided in the supplementary material for reproducibility of the results.

Using simulation, the optimal constant, control limits, decision outcome and total decision cost of the original (Shewhart) and risk-based $\bar{X}$ charts for different sample sizes (n) are obtained and reported in Table 3. In Table 3, 'O' denotes the traditional/original

Algorithm 2 Pseudocode for the RB chart in Phase II analysis

1: **Input:** obs, n, μ_X, va_X, sk_X, ku_X, μ_e, va_e, C, δ, LCL, UCL, LCL_{rb}, UCL_{rb}
2: Generate true process data $X \leftarrow$`generate(obs,` μ_X `,` va_X `,` sk_X `,` ku_X `,` δ`)`
3: Generate measurement error data $UC \leftarrow$ `data_gen(obs,` μ_e `,` va_e `, 0, 3)`
4: Define a cost function $f(C) \leftarrow$ total cost from `phase2 (obs, n, X,UC, C, LCL, UCL,` LCL_{rb} `,` UCL_{rb} `,` δ`)`
5: **Output:** total cost (TC_{in} or TC_{out}), decision cost of outcomes (C_{11}, C_{10} or C_{01}, C_{00}), cost ratio (CR_0 or CR_1), probability ratio (PR_0 or PR_1 accordingly.

Table 2
Simulation parameters.

Notation	Definition	Value
μ_x	Process expected value	10
σ_x	Process standard deviation	0.5
σ_e	Standard deviation of measurement uncertainty	0.05
m	Number of data observations generated	1000
n	Sample size	(1,2,3,4,5,8)
r	Number of simulations for each chart	100
c_{11}	Cost of correct acceptance	1
c_{10}	Cost of incorrect control	5
c_{01}	Cost of incorrect acceptance	60
c_{00}	Cost of correct control	5
α	level of significance in Shewhart scheme	0.0027

Table 3
Control limits, decision results, and overall decision cost in Phase I.

n	Type	k	LCL	UCL	q_{11}	q_{10}	q_{01}	q_{00}	TC
1	O	3	8.49	11.51	997.1	0.3	0.2	2.4	1024.8
	RB	2.95	8.51	11.49	996.8	0.6	0	2.6	1012.8
2	O	3	8.94	11.06	996.8	0.4	0.4	2.3	1035.1
	RB	2.95	8.95	11.05	996.1	1.1	0	2.7	1015.4
3	O	3	9.13	10.86	997.2	0.3	0.2	2.2	1024.4
	RB	2.97	9.14	10.85	996.9	0.6	0	2.5	1012.1
4	O	3	9.25	10.75	996.9	0.4	0.3	2.3	1030.2
	RB	2.94	9.26	10.74	996.5	0.9	0	2.7	1014.1
5	O	3	9.32	10.67	996.8	0.3	0.4	2.5	1032.4
	RB	2.96	9.33	10.66	996.5	0.6	0	2.8	1014.5
8	O	3	9.46	10.53	997.2	0.3	0.3	2.2	1025.4
	RB	2.94	9.48	10.52	996.8	0.7	0	2.5	1012.9

charts, and 'RB' denotes the risk-based $\bar{X}$ charts. To visualize the results, boxplot diagrams for each type are constructed at different n values and are provided in Fig. 1. The vertical axes of the figure display the median and distribution of the overall cost for both strategies over a range of n values.

Table 3 shows that the risk-based strategy reduces the overall cost of the process through optimization and outperforms the conventional chart does. An identical conclusion can be drawn in Fig. 1. Furthermore, the mean values of the charting constant (k) decrease following optimization. Optimization reduces the control area to avoid false acceptance, as type II errors result in far more severe outcomes (i.e., substantially higher decision costs), and both type I and type II errors are balanced in the risk-based chart, as evident in Table 3. The error counts for type I and type II were lower for the risk-based type than for the original type $\bar{X}$ chart. The results likewise do not indicate any connection between sample size and an ideal value of K. Similar conclusions can be drawn regarding the overall decision cost, which does not vary with changes in sample size. These results support the findings of Katona et al. [40].

Phase II analysis

Phase II analysis is usually implemented in SPC to monitor the process using control limits established in Phase I and detect shifts in the process over time [1]. The performance of the risk-based chart (designed on the basis of the Phase I samples) is evaluated here for a Phase II sample generated under H_0 and H_a. The real and measurement error values are again simulated as Phase II data, and the control limits given in Table 3 are deployed to estimate the conditional decision outcomes, total decision cost, CR, PR and ARL. The findings for $\delta = 0$ are shown in Table 4.

Table 4 shows that the conditional total decision cost (TC) of the $\bar{X}$ chart for both types (original and risk-based) is almost equal when the process is in control. Additionally, the cost ratio (CR) is slightly different for both approaches but is not significant, but the ARL for both approaches is significantly different than the fixed value of ARL_0=370 (usually set). Both approaches produce

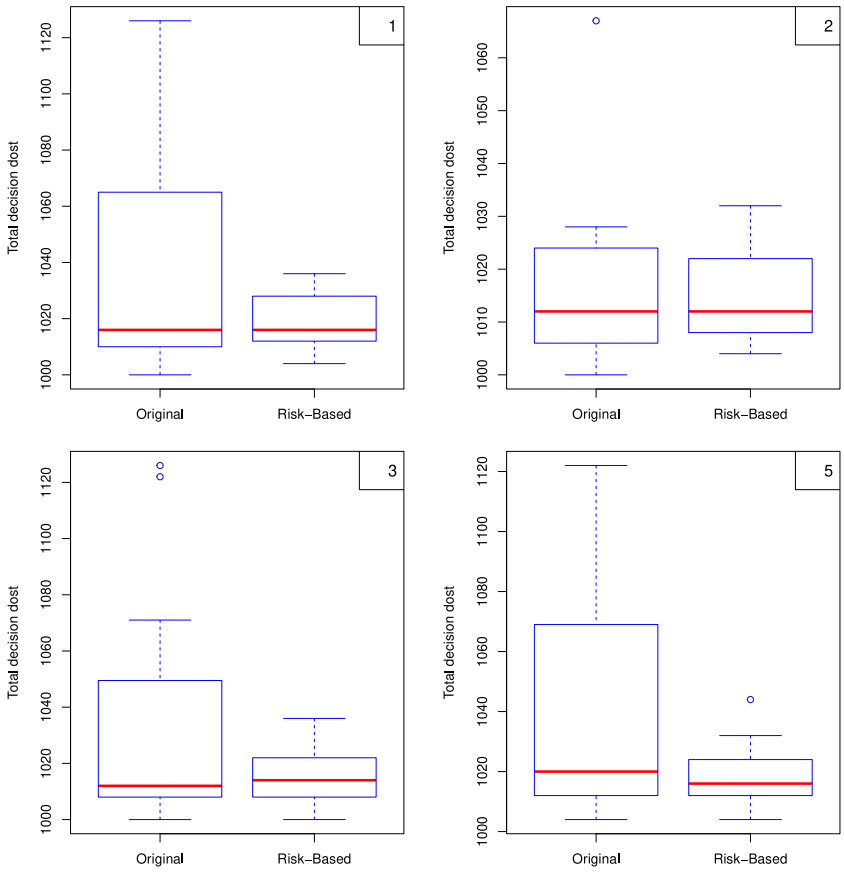

Fig. 1. Distribution of the simulation's total cost for $n = 1$, 2, 3, or 5 in Phase I.

Table 4
Phase II conditional performance of the $\bar{X}$ chart when $\delta = 0$.

n	Type	q_{11}	q_{10}	TC	CR	PR	ARL
1	O	997.1	0.3	998.5	0.0015	0.0003	3333
	RB	996.8	0.6	999.7	0.0030	0.0006	1667
2	O	996.7	0.4	998.9	0.0020	0.0004	2500
	RB	996.5	0.6	999.5	0.0030	0.0006	1667
3	O	997.2	0.4	999.3	0.0020	0.0004	2500
	RB	996.9	0.7	1000.2	0.0035	0.0007	1428
5	O	996.9	0.4	998.9	0.0020	0.0004	2500
	RB	996.7	0.6	999.9	0.0030	0.0006	1667

smaller associated type I errors (underestimating the desired $\alpha = 0.0027$). This discrepancy arises from how parameter estimation affects the efficacy of $\bar{X}$, as examined by numerous scholars, including [51–53]. Although this issue can be addressed via "the guaranteed in-control performance approach" (see [52]), it is not considered here. Among the compared approaches, the risk-based approach is the least affected by parameter estimation. In this study, the limits are estimated on the basis of 25 samples. Moreover, no relationship between sample size and the in-control performance indicators is observed.

Additionally, the conditional effectiveness of the considered chart is checked when the process deviates from control. The conditional decision outcomes, total decision cost, CR, PR, ARL and p^* are calculated for $\delta = 0.5, 1.0, 1.5, 2.0$ and reported here in Tables 5–7 when n = 1,2,3. To visualize the results, boxplot diagrams of the Phase II conditional distribution of total decision cost are constructed for $\delta = 1, 1.5$ and n = 1,2, as shown in Fig. 2. The total decision cost curves and ARL curves for various values of δ and $n = 1, 2$ in the Phase II analysis are presented in Fig. 3 and Fig. 4, respectively.

The results of Tables 5–7 imply that when $\delta \neq 0$:

Table 5
Phase II conditional performance of the $\bar{X}$ chart when $\delta \neq 0$ and $n = 1$.

δ	type	q_{01}	q_{00}	TC_{out}	CR	PR	ARL	p^*
0.5	O	0.5	5.1	54.7	1.17	0.15	185.18	0.0000
	RB	0.3	5.3	44.3	0.68	0.09	172.41	0.0000
1. 0	O	2.1	19.6	221.5	1.28	0.11	51.02	0.0004
	RB	1.3	20.4	177.5	0.76	0.06	49.01	0.0004
1. 5	O	4.6	60.8	576.9	0.90	0.08	16.45	0.0040
	RB	2.6	62.7	470.2	0.49	0.04	15.95	0.0041
2. 0	O	9.1	146.5	1281.0	0.74	0.06	6.84	0.0228
	RB	5.3	150.3	1072.0	0.42	0.03	6.65	0.0234

Table 6
Phase II conditional performance of the $\bar{X}$ chart when $\delta \neq 0$ and $n = 2$.

δ	Type	q_{01}	q_{00}	TC_{out}	CR	PR	ARL	p^*
0.5	O	0.9	10.5	110.6	1.03	0.09	95.24	0.0001
	RB	0.6	10.8	92.5	0.67	0.06	92.59	0.0001
1. 0	O	4.0	52.9	506.1	0.91	0.08	18.90	0.0030
	RB	3.0	54	450.6	0.67	0.06	18.52	0.0031
1. 5	O	10.3	179.9	1516.9	0.69	0.06	5.56	0.0196
	RB	7.1	183.1	1339.8	0.46	0.04	5.46	0.0199
2. 0	O	15.7	417.3	3029.1	0.45	0.04	2.39	0.1807
	RB	1.7	422.3	2755	0.05	0.02	2.37	0.1829

Table 7
Phase II conditional performance of the $\bar{X}$ chart when $\delta \neq 0$ and $n = 3$.

δ	Type	q_{01}	q_{00}	TC_{out}	CR	PR	ARL	p^*
0.5	O	1.4	14.9	157.1	1.13	0.10	67.11	0.0002
	RB	0.9	15.4	134	0.70	0.06	64.94	0.0002
1. 0	O	6.6	99.9	896.2	0.79	0.07	10.01	0.0106
	RB	4.2	102.3	766.4	0.49	0.04	9.80	0.0109
1. 5	O	14.0	337.3	2529	0.50	0.04	2.96	0.1185
	RB	8.6	342.7	2232.2	0.30	0.02	2.91	0.1204
2. 0	O	14.2	671	4207	0.25	0.02	1.49	0.4597
	RB	8.7	676.5	3906.1	0.15	0.01	1.47	0.4635

- The RB chart outperforms the original chart in terms of decreased conditional total decision cost (TC_{out}) across all sample sizes. This is similarly illustrated in Fig. 2. The number of type II errors decreases while the number of correct rejections increases for the RB approach at different values of n.
- The value of TC_{out} for each type of chart increases as n increases for a fixed value of δ. Additionally, this can be seen in Fig. 3. This is because a larger number of inspection units leads to an increase in the overall inspection costs.
- The RB chart also outperforms the original chart in terms of the decrease in the conditional decision cost ratio (CR) for a given sample size. A high CR indicates that the cost of making an incorrect acceptance decision is greater than that of making a correct rejection. The occurrence of type II errors decreases while the number of correct rejections increases in the RB approach, causing a reduction in the CR value. This conclusion holds for all sample sizes.
- The RB chart also outperforms the original chart when the probability ratio (PR) is considered. A high PR value suggests that the likelihood of making an incorrect acceptance decision exceeds that of making a correct rejection at a constant value of n. This is attributed to a reduced incidence of type II errors and an increased number of correct rejections resulting from the RB approach. These findings are consistent across all sample sizes.
- Compared with the original chart, the RB chart shows enhanced ARL performance for all sample sizes. Fig. 4 also implies the same pattern. A reduction in the ARL value indicates improved ARL performance as the value of n increases, which is in line with earlier research. (see [1,3,6,52]).
- For all sample sizes, the RB chart displays improved overall signal performance compared to the original chart. Additionally, when δ is fixed, the likelihood of signals (p^*) increases as n increases.

In general, the risk-based $\bar{X}$ chart outperforms the original $\bar{X}$ chart concerning TC, CR, PR, and ARL in identifying a shift more rapidly during out-of-control situations. If the process is out of control, a higher conditional total cost results in smaller ARL values because a greater number of correct rejections results in a greater associated cost and fewer samples to signal a shift. These findings demonstrate the advantages of using the risk-based approach in process improvement under measurement uncertainty.

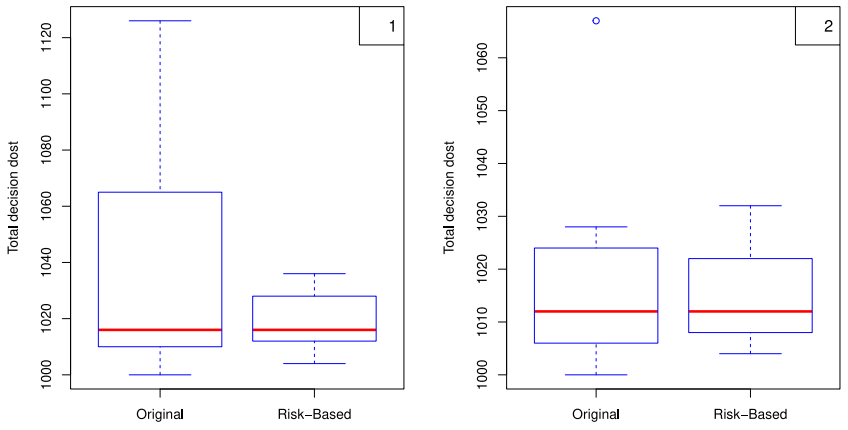

(a) $\delta = 1$

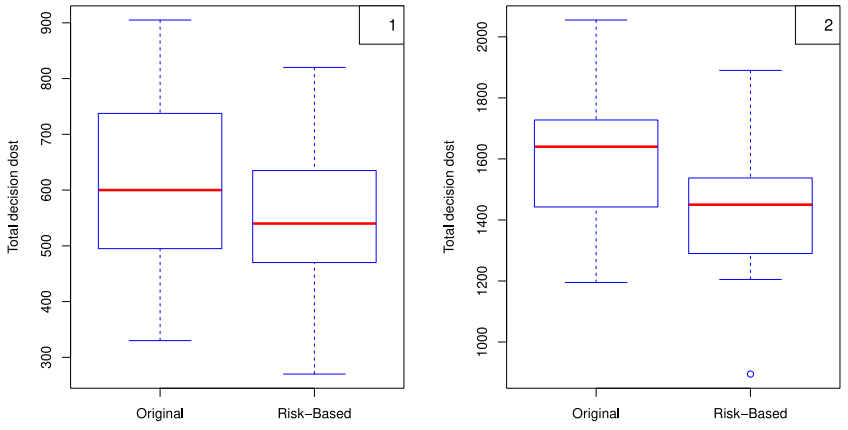

(b) $\delta = 1.5$

Fig. 2. Distribution of the total conditional decision cost for $\delta = 1{,}1.5$ and $n = 1{,}2$.

4.2. Evaluation through a real dataset

The efficacy of the risk-based $\bar{X}$ graphic is additionally assessed via a real dataset developed by Katona [16] and examined by Katona et al. [40]. We use the same dataset to demonstrate how to implement the proposed design step by step in practice. The selected product was master brake cylinders manufactured by the automotive industry (cf., [54]). Two product characteristics (attributes) were examined: cutting length (the full-stroke length of the piston) and core diameter (internal bore diameter). These two components play important roles in the manufacturing quality, performance, and cost efficiency of a master brake cylinder [55,56]. The dataset is available in the *rbcc* package with the name *t2uc* (). In the dataset, each attribute was measured twice via a 3D optical scanner and a manual height gauge (caliper). The 50 measurements were recorded with 1 product each time. The "true" values (indicated as x) signify the accurate measurement of the cutting length via a 3D optical scanner, whereas the "measured" value (denoted as y) is derived via a manual height gauge (caliper). Following the values of x and y, the measurement error was also calculated with the simple additive model given in Eq. (6) for each ith measurement. The finance department estimated the expenses of the four possible outcomes as $C = (1, 20, 160, 5)$ [16].

To demonstrate the application of the $\bar{X}$ chart, we consider the cutting length as a quality characteristic to be monitored in this automotive manufacturing process [16]. In practice, a change in the mean cutting length and an increase or decrease in the average length of material being cut during machining can directly impact the quality, consistency, and reliability of a master brake cylinder [56]. Using these realizations, we subsequently implement the suggested plan to track the cutting length and identify any variations in the process average. The following are the specific implementation steps.

Step 1: Estimate the mean and standard deviation of the real values (x) and observed values (y) on the basis of the Phase-I data. We obtain an average of 84.49 and a standard deviation of 0.07 for "real" values, whereas "observed" values have a mean of 84.54 and a standard deviation of 0.08. Thus, the estimated characteristics of the data highlight that measurement uncertainty exists in a 3D optical scanner.

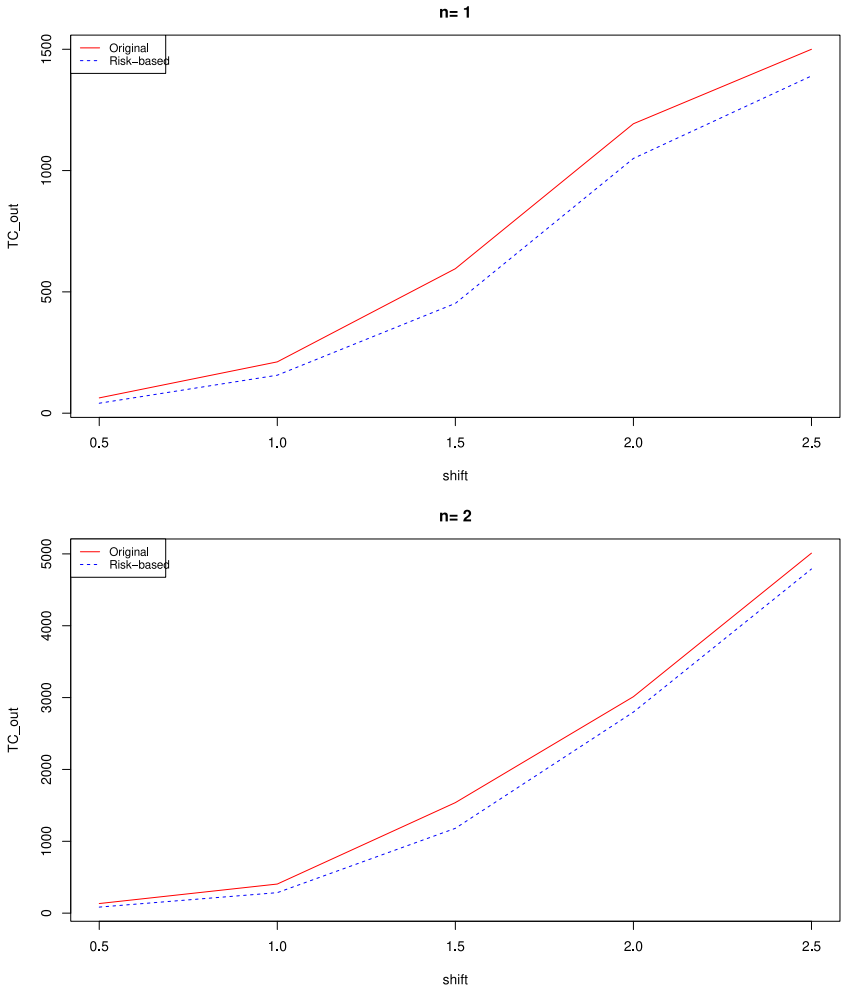

Fig. 3. Total decision cost curves for different shift sizes at $n = 1$ and 2.

Table 8
Limits, decisions, and the overall cost of decisions on an actual dataset.

Type	k	LCL	UCL	q_{11}	q_{10}	q_{01}	q_{00}	TC
O	3	84.30	84.70	48	2	0	0	88
RB	3.82	84.24	84.75	50	0	0	0	50

Step 2: Choose the desired n, IC ARL, and cost structure C. Determine the control limits and k on the basis of $n = 1$, and the IC ARL=370 using the original Shewhart-based approach. Start monitoring the average of the cutting length process and obtain plotting statistics $\bar{X}$ in Eq. (1) for x_i and y_i, $i = 1, 2, \ldots, 50$. These are compared with the standard control limits, and each decision outcome and overall cost of the process are calculated using Eq. (7). Optimize the total cost function for the optimum value of k via the Nelder–Mead algorithm.

Consequently, we obtained the results given in Table 8. The outcome of Table 8 aligns with the findings of Katona et al. [40]. Finally, we construct the original and proposed risk-based $\bar{X}$ charts on the cutting length data, as shown in Fig. 5. The "real" process is shown by the black lines, whereas the "measure" sample values are represented by the blue lines. Both the observed and real data were used to create the control lines, which are shown as dashed lines. Finally, the green dots indicate Type 1 errors. As shown in Fig. 5, the process works within the specifications using a risk-based methodology approach (which incorporates the measurement uncertainty) because no points fall outside the actual control lines (blue). The application of the original approach (which does not consider measurement uncertainty in the design) produces two incorrect signals (type I errors) on the basis of the observed measurements. These signals are not due to a shift but are due to incorrect measurements.

Step 3: Implementation of the risk-based design in Phase II analysis requires the out-of-control samples of the master brake cylinder. Collecting out-of-control samples from actual production processes in industry can be expensive and difficult. Therefore, we

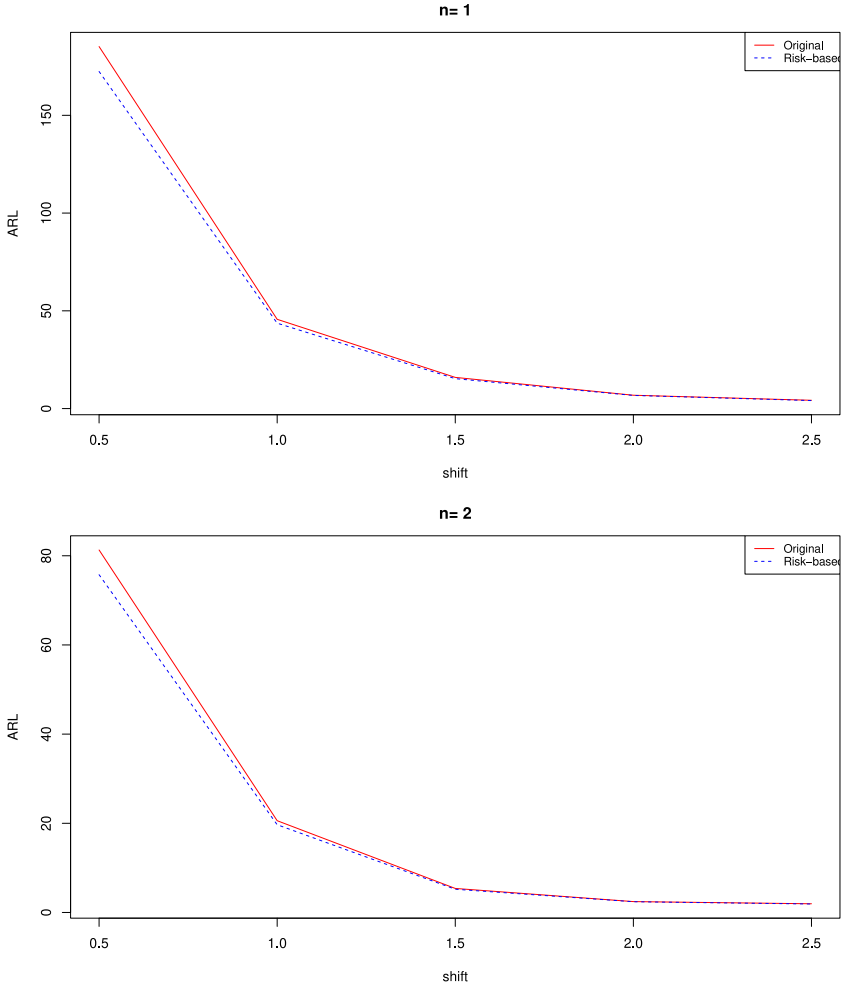

Fig. 4. ARL curves for different shift sizes at $n = 1$ and 2.

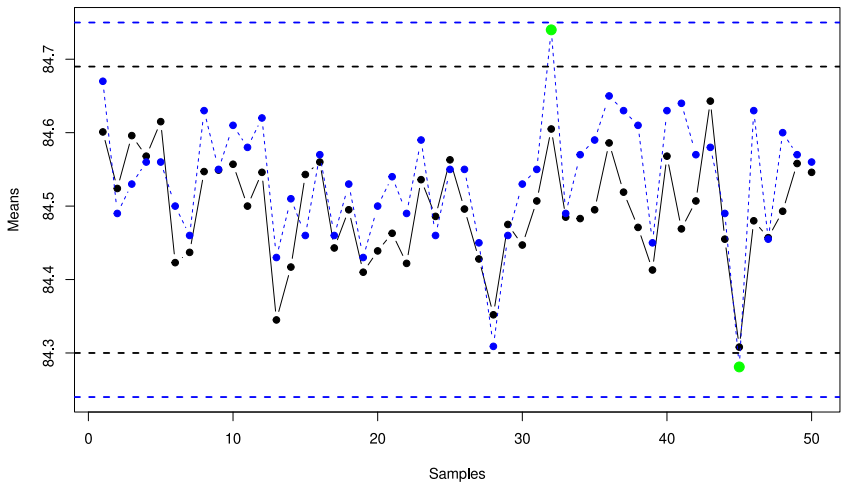

Fig. 5. $\bar{X}$ charts showing actual and estimated processes for Phase-I in-control data.

Table 9
Phase-II measurements after $\delta = 1$ and plotting statistics for the actual dataset.

j	x_j	ϵ_j	y_j	j	x_j	ϵ_j	y_j	j	x_j	ϵ_j	y_j
1	84.671	0.069	84.740	18	84.565	0.035	84.600	35	84.565	0.095	84.660
2	84.594	−0.034	84.560	19	84.480	0.020	84.500	36	84.656	0.064	84.720
3	84.666	−0.066	84.600	20	84.509	0.061	84.570	37	84.589	0.111	84.700
4	84.638	−0.008	84.630	21	84.533	0.077	84.610	38	84.541	0.139	84.680
5	84.685	−0.055	84.630	22	84.492	0.068	84.560	39	84.483	0.037	84.520
6	84.493	0.077	84.570	23	84.606	0.054	84.660	40	84.638	0.062	84.700
7	84.507	0.023	84.530	24	84.556	−0.026	84.530	41	84.539	0.171	84.710
8	84.617	0.083	84.700	25	84.633	−0.013	84.620	42	84.577	0.063	84.640
9	84.619	0.001	84.620	26	84.566	0.054	84.620	43	84.713	−0.063	84.650
10	84.627	0.053	84.680	27	84.498	0.022	84.520	44	84.525	0.035	84.560
11	84.570	0.080	84.650	28	84.422	−0.043	84.379	45	84.378	−0.027	84.351
12	84.616	0.074	84.690	29	84.545	−0.015	84.530	46	84.550	0.150	84.700
13	84.415	0.085	84.500	30	84.517	0.083	84.600	47	84.527	−0.002	84.525
14	84.487	0.093	84.580	31	84.577	0.043	84.620	48	84.563	0.107	84.670
15	84.613	−0.083	84.530	32	84.675	0.135	84.810	49	84.628	0.012	84.640
16	84.630	0.010	84.640	33	84.555	0.005	84.560	50	84.616	0.014	84.630
17	84.513	0.017	84.530	34	84.553	0.087	84.640				

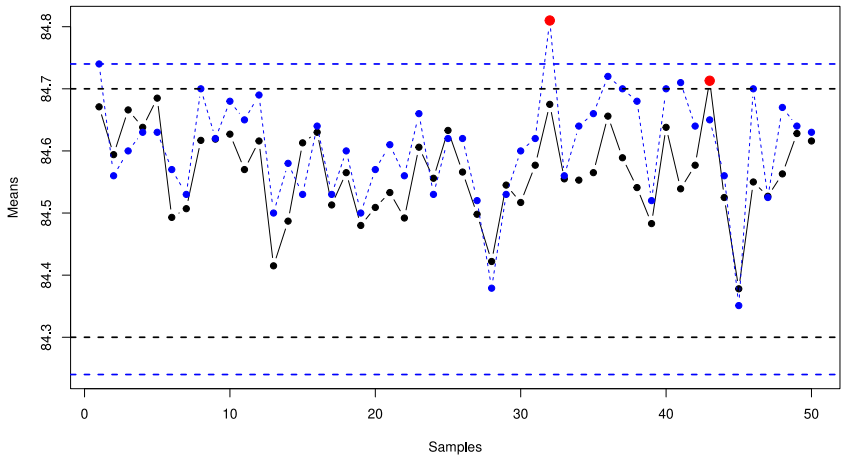

Fig. 6. $\bar{X}$ charts showing actual and estimated processes for $\delta = 1$.

purposefully add a shift of 1σ to the true measurements ($x+0.07$) to manufacture the OC samples. The Phase-II x_j and corresponding y_j with ϵ_j for j = 1, …, 50 and $n = 1$ are displayed in Table 9. Since individual values have been accounted for, the plotting statistics $\bar{X}_j = x_j$ and $\bar{Y}_j = y_j$ are used.

Step 4: The mean of the Phase-II true measurements is 84.566, which is shifted from the in-control mean μ_0 by 1σ times (i.e., $\mu_1 = \mu_0 + 1\sigma$). The mean control chart for Phase-II analysis using the traditional and risk-based approaches to determine the detectability is constructed in Fig. 6. The black and blue lines have the same meanings as in the description in Fig. 5, and the red dots indicate whether proper rejection occurred (shift detected). The 'RB' mean chart detects the process shift (at the 32nd sample) earlier than the 'O' mean chart (at the 43rd sample) even a smaller shift ($\delta = 1$), as shown in Fig. 6. Such a rise in the average level suggests an intolerable component mismatch, which could be caused by incorrect sensor alignment, surface reflectivity, vibration, etc., preventing the components from self-adjusting appropriately. The manufacturing process needs to be reexamined.

Step 5: After correctly identifying the out-of-control reasons and fixing the problem, we return to Step 1 to revise the design of the chart and restart the monitoring procedure for the manufacturing process.

5. Sensitivity analysis

The applicability of the risk-based $\bar{X}$ chart depends on several parameters, as outlined in the preceding section, when $\delta = 0$. The sensitivity analysis looks at the effects of the following parameters.

- Sample size (n)
- Decision cost of correct rejection (c_{00})
- Shift size (δ)
- standard deviation (σ_{UC})

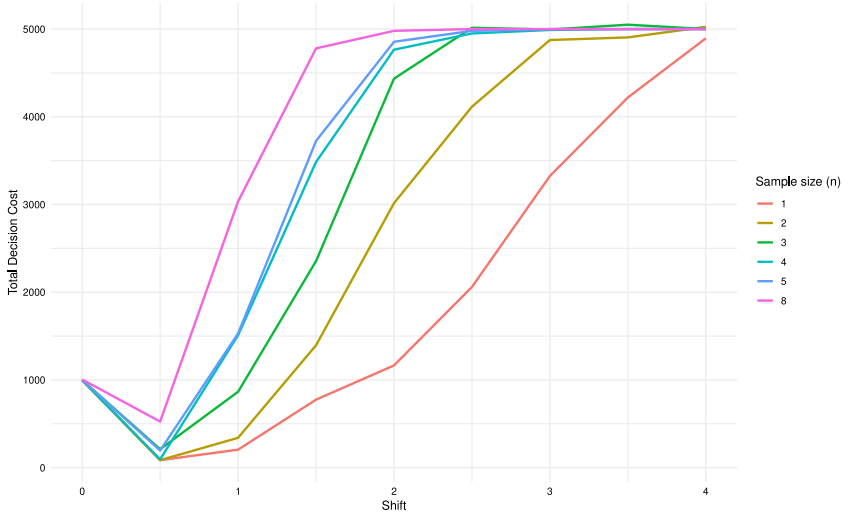

Fig. 7. Analysis of sensitivity for n.

These parameters were selected because of their significant influence on the chart's out-of-control behavior. The expense of correct rejection could influence the feasibility of the control policy. The chart's effectiveness can be assessed by examining the sample size, the shift magnitude, and the standard deviation of the product measurement inaccuracies. In the sensitivity analysis, we examine the identical simulation parameters listed in Table 2 with a few alterations.

5.1. Sample size (n)

When any control charts are used, the sample size is an important consideration. A larger sample size yields a more accurate assessment of the production process, but it also increases production costs. Furthermore, the performance metrics are significantly affected by the sample size. The overall decision cost is used to evaluate the performance of the risk-based chart for different sample sizes. Simulation is used to assess how the sample size affects the overall decision cost of the process for different shift sizes ($\delta = 0, 0.5, \ldots, 4$). Fig. 7 displays the simulation outcomes. For a given shift size, the total decision cost increased dramatically as the sample size increased. However, as shown in Fig. 7, the overall cost of the decision is not significantly affected by larger sample sizes or shift sizes. These findings indicate that, especially for small to moderate shift sizes, the performance of a risk-based chart is sensitive to changes in sample size (n).

5.2. Cost of correct rejection (c_{00})

The risk-based design minimizes the cost of Type II errors (c_{01}) during the control process and increases the cost of correct decisions (c_{00}). Therefore, it is essential to examine the connection between the cost of the correct decision, the total cost of the decision, and the size of the change (δ). During the analysis, c_{00}, δ, and σ_{uc} vary, whereas the other parameters remain unchanged. The ratio of the cost of proper rejection to the cost of incorrect acceptance is represented by values of c_{00}. The results are presented in Fig. 8 for $n = 2$. The x-axis in the figure represents the values of c_{00}, the y-axis represents the overall cost of the decision, the color 'lines' represents the values of δ ranging from 0–3, and each subfigure (panel) is constructed at the given value of σ_{uc} (ve) ranging from 0.5–5. These settings are also considered in the following figures.

Fig. 8. reveals that (i) for a fixed value of $\delta > 0$ and σ_{uc}, TC increases with increasing c_{00}; (ii) for a fixed value of σ_{uc}, TC increases with increasing c_{00} and δ; and (iii) at a given value of δ, TC increases with increasing c_{00} and σ_{UC}. Thus, a higher value of the correct rejection cost increases the total number of decisions (TC). A higher correction decision can be made by reducing type II errors, but this entails a strict control policy.

5.3. Shift size (δ)

Control charts of the Shewhart type help identify significant changes, whereas memory-based control charts (EWMA, CUSUM, and MA charts) are better at spotting minute changes in the process parameter(s). Consequently, the magnitude of the shift greatly impacts the assessment of control charts. Various shift sizes (from small to large) are considered, and the overall decision cost is used to assess the $\bar{X}$ chart's statistical performance. The simulation outcomes are shown in Fig. 9.

For a fixed value of c_{00} and σ_{uc}, TC increases when the shift size (δ) increases, and at a given value of σ_{uc}, TC likewise increases as c_{00} and δ increase. These results verify the detectability of the risk-based chart for minor to major process changes.

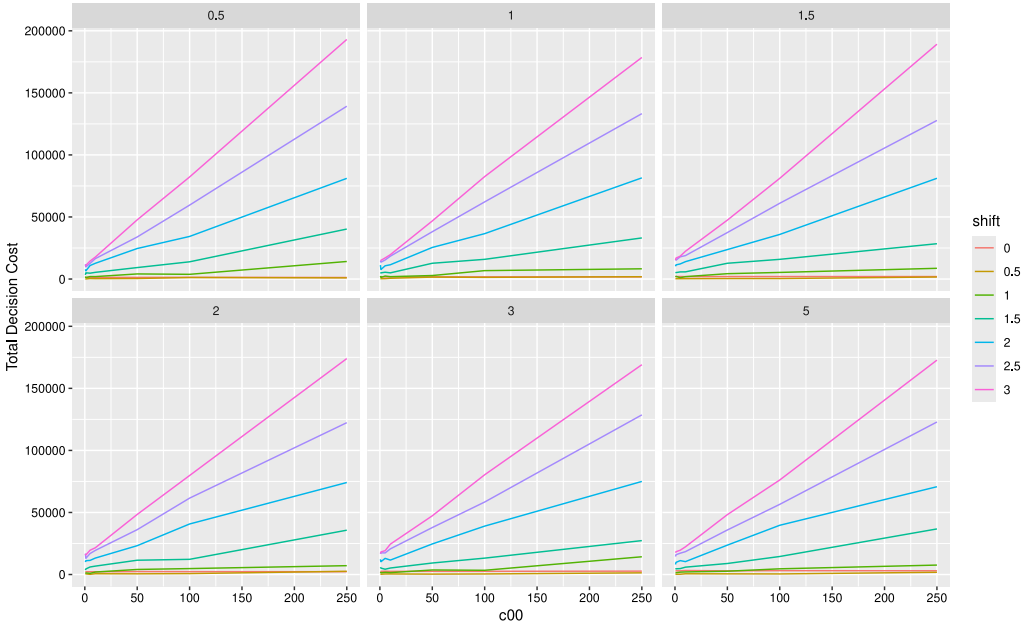

Fig. 8. Sensitivity analysis for the cost of correct rejection.

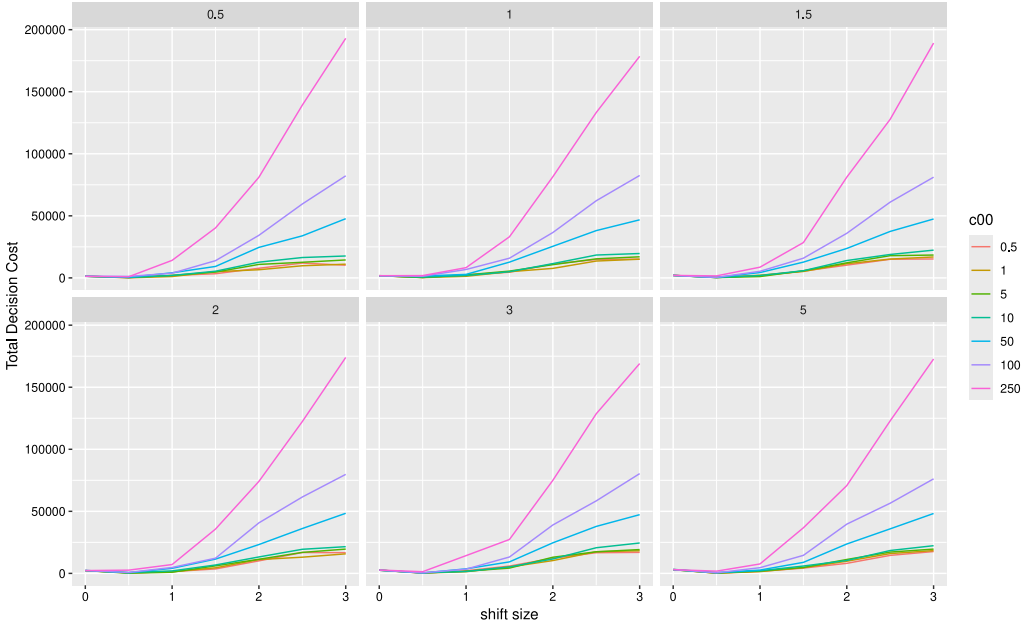

Fig. 9. Sensitivity analysis for shift size.

5.4. Measurement error (σ_{UC})

The out-of-control behavior of the risk-based chart may also be influenced by the standard deviation of the measurement error. Therefore, if the uncertainty in the measurement can be defined, its impact can be simulated during the design and assessment of a risk-based chart. The efficiency of the risk-based chart is also examined, as σ_{UC} related to the process increases here. Fig. 10 displays the outcomes of this analysis for $n = 2$.

For a given value of c_{00} and δ, the value of σ_{UC} does not significantly affect the total conditional decision cost of an out-of-control process except for a very high cost of correct acceptance ($c_{00} \geq 100$) or/and a large shift size ($\delta \geq 2$), as is obvious from Fig. 10. Thus,

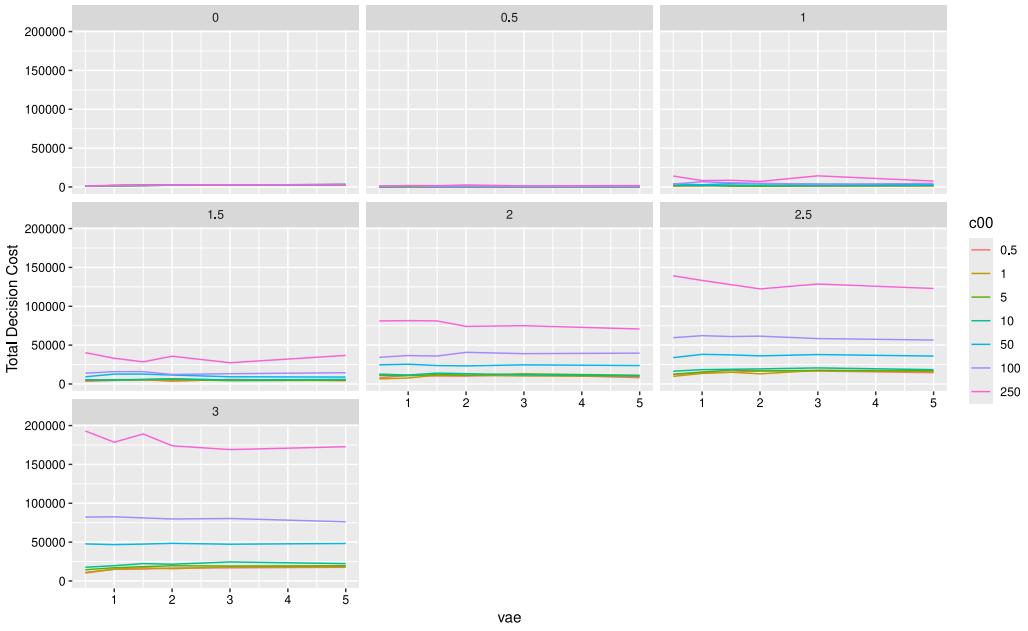

Fig. 10. Analysis of sensitivity for measurement error (σ_{UC}).

the performance of the risk-based $\bar{X}$ chart shows little sensitivity to the standard deviation of the measurement error, particularly for minor changes.

6. Conclusions

In a more industrialized setting, the precision of measurements is crucial. Measurement uncertainty should be acknowledged and considered when decisions are being made. Consequently, it is crucial to create process control strategies that consider measurement uncertainty and the outcomes of decisions. To address measurement uncertainty, [38–40] presented a novel family of control charts (risk-based charts) for the SPC. Nonetheless, neither in-control nor out-of-control scenarios have been utilized to assess the statistical effectiveness of risk-based charts. The efficacy of the risk-based control chart under in-control and out-of-control conditions with measurement uncertainty was a crucial factor in addition to its design. The primary objective of this study was to analyze the effectiveness of risk-based control charts in both in-control and out-of-control scenarios that consider measurement uncertainty in performance metrics.

A univariate risk-based chart $\bar{X}$ is analyzed to assess its statistical effectiveness amid measurement uncertainty. The performance under conditional circumstances is assessed for the SPC's in-control and out-of-control states. Assessment is performed not only in simulated scenarios but also in actual circumstances. Furthermore, we believe that improving the correct rejection rate and reducing the average number of samples needed before shift detection can be effortlessly achieved through the use of risk-based control charts. The results reveal that the risk-based average control chart minimizes the overall decision cost of the process when the process is in a state of in-control and correctly identifies the changes when the process is out-of-control.

The primary contributions of this paper are listed below. First, the relevance of the risk-based method is greatly enhanced by examining its statistical effectiveness in identifying a change in the SPC (C_1). This work opens new room for the development of family risk-based charts via a statistical design such as a guaranteed in-control approach [52], a percentile-based approach [57], etc. Second, the increase in correct rejection decision costs and decrease in ARL (early signal) can be attained with average charts (C_2). This suggests that companies dealing with simple processes can leverage risk-based charts to lower total decision costs, enhance correct rejection, and identify early signals. Third, validating the statistical assessment of a risk-based graph via practical data underscores the importance of its practical application in balancing the risks faced by producers and consumers in the SPC (C_3). Fourth, the practitioner is guided in selecting the necessary parameters for the risk-based charts in the SPC application via sensitivity analysis of the relevant parameters (C_4).

One future study is an integration of EWMA with the proposed model, and the authors are working in this direction. Other future research avenues include the statistical design and assessment of more risk-based charts.

Funding

This work has been implemented by the TKP2021-NVA-10 and BME-NVA-02 projects, with support provided by the Ministry of Culture and Innovation of Hungary from the National Research, Development and Innovation Fund, financed under the 2021 Thematic Excellence Programme funding scheme.

Declaration of competing interest

The authors declare that they have no known competing financial interests or personal relationships that could have appeared to influence the work reported in this paper.

Data availability

Data will be made available on request.

References

[1] Montgomery DC. Introduction to statistical quality control. John wiley & sons; 2019.
[2] Shewhart WA. Economic control of quality of manufactured product. Macmillan And Co Ltd, London; 1931.
[3] Aslam M, Saghir A, Ahmad L. Introduction to statistical process control. John Wiley & Sons; 2020.
[4] Alsaid M, Kamal RM, Rashwan MM. The performance of control charts with economic-statistical design when parameters are estimated. Rev Econ Political Sci 2021;6(2):142–60.
[5] Yu S, Wan Q, Wei Z, Tang T. Statistical design of an adaptive synthetic X-Control chart with run rule on service and management operation. Sci Program 2016;2016(1):9629170.
[6] Madzík P, Krizo P. The effect of nonnormal distributions on the control limits of X-bar chart. Proc Int Sci Days 2018;851–62.
[7] Oviedo-Trespalacios O, Peñabaena-Niebles R. Statistical performance of control charts with variable parameters for autocorrelated processes. Dyna 2016;83(197):120–7.
[8] Shongwe SC, Malela-Majika J-C, Molahloe T. One-sided runs-rules schemes to monitor autocorrelated time series data using a first-order autoregressive model with skip sampling strategies. Qual Reliab Eng Int 2019;35(6):1973–97.
[9] Duncan AJ. The economic design of x charts used to maintain current control of a process. J Amer Statist Assoc 1956;51(274):228–42.
[10] Quintero-Arteaga C, Peñabaena-Niebles R, Vélez JI, Jubiz-Diaz M. Statistical design of an adaptive synthetic X-bar control chart for autocorrelated processes. Qual Reliab Eng Int 2022.
[11] Safaei AS, Kazemzadeh RB, Gan H-S. Robust economic-statistical design of X-bar control chart. Int J Prod Res 2015;53(14):4446–58.
[12] Amiri F, Noghondarian K, Noorossana R. Economic-statistical design of adaptive X-bar control chart: a Taguchi loss function approach. Sci Iran 2014;21(3):1096–104.
[13] Elahi B, Deheshvar A, Franchetti M, Amiri Tokaldany S. Optimum evaluation performance of adaptive X-bar control charts. J Ind Prod Eng 2022;39(8):644–53.
[14] Giri B. Managing inventory with two suppliers under yield uncertainty and risk aversion. Int J Prod Econ 2011;133(1):80–5.
[15] Lira I. A Bayesian approach to the consumer's and producer's risks in measurement. Metrologia 1999;36(5):397.
[16] Katona A. Validation of risk-based quality control techniques: a case study from the automotive industry. J Appl Stat 2021;1–20.
[17] Golosnoy V, Hildebrandt B, Köhler S, Schmid W, Seifert MI. Control charts for measurement error models. AStA Adv Stat Anal 2023;107(4):693–712.
[18] Pendrill LR. Operating 'cost'characteristics in sampling by variable and attribute. Accrédit Qual Assur 2008;13(11):619–31.
[19] Peruchi RS, Balestrassi PP, de Paiva AP, Ferreira JR, de Santana Carmelossi M. A new multivariate gage R&R method for correlated characteristics. Int J Prod Econ 2013;144(1):301–15.
[20] Abraham B. Control charts and measurement error. In: Annual technical conference of the American society for quality control. vol. 31, 1977, p. 370–4.
[21] Asif F, Khan S, Noor-ul Amin M. Hybrid exponentially weighted moving average control chart with measurement error. Iran J Sci Technol Trans A: Sci 2020;44(3):801–11.
[22] Hu X, Castagliola P, Sun J, Khoo MB. The performance of variable sample size chart with measurement errors. Qual Reliab Eng Int 2016;32(3):969–83.
[23] Linna KW, Woodall WH, Busby KL. The performance of multivariate control charts in the presence of measurement error. J Qual Technol 2001;33(3):349–55.
[24] Maravelakis PE. Measurement error effect on the CUSUM control chart. J Appl Stat 2012;39(2):323–36.
[25] Sabahno H, Amiri A, Castagliola P. Performance of the variable parameters X control chart in presence of measurement errors. J Test Eval 2018;47(1):480–97.
[26] Saghaei A, Fatemi Ghomi S, Jaberi S. Economic design of exponentially weighted moving average control chart based on measurement error using genetic algorithm. Qual Reliab Eng Int 2014;30(8):1153–63.
[27] Aslam M. Design of X-bar control chart for resampling under uncertainty environment. IEEE Access 2019;7:60661–71.
[28] Zaidi FS, Castagliola P, Tran KP, Khoo MBC. Performance of the MEWMA-CoDa control chart in the presence of measurement errors. Qual Reliab Eng Int 2020;36(7):2411–40.
[29] Jawad Mirza M, Hashmi S, Thomas Mwakudisa M, Safariyan A, Naghmi Habibullah S, Noor-ul Amin M. Performance evaluation of extended EWMA control chart in the presence of measurement error. Comm Statist Simulation Comput 2024;1–16.
[30] Carrillo R, Minutti C, Lagunes P. A comprehensive methodology for performing continued process verification. In: 2024 IEEE 37th international symposium on computer-based medical systems. IEEE; 2024, p. 284–9.
[31] Shojaee M, Noori S, Jafarian-Namin S, Hassanvand F, Johannssen A. Designing economic-statistical hotelling's T 2 control charts for monitoring linear profiles under uncertainty of parameters. J Stat Comput Simul 2024;94(18):4019–36.
[32] Ahmadini AAH, Khan I, Alshqaq SSA, AlQadi H, Ghodhbani R, Ahmad B. Improved adaptive CUSUM control chart for industrial process monitoring under measurement error. Sci Rep 2025;15(1):16616.
[33] Jafarian-Namin S, Fattahi P, Salmasnia A. Assessing the economic-statistical performance of variable acceptance sampling plans based on loss function. Comput Statist 2024;1–49.
[34] Kosztyán ZT, Csizmadia T, Hegedűs C, Kovács Z. Treating measurement uncertainty in complete conformity control system. In: Innovations and advances in computer sciences and engineering. Springer; 2010, p. 79–84.
[35] Hegedűs C, Kosztyán ZT. The consideration of measurement uncertainty in forecast and maintenance related decisions. Probl Manag 21st Century 2011;1:46.
[36] Kosztyán ZT, Hegedűs C, Katona A. Treating measurement uncertainty in industrial conformity control. Central Eur J Oper Res 2017;25(4):907–28.
[37] Hegedűs C, Kosztyán ZT, Katona A. Parameter drift in risk-based statistical control charts. Glob J Technol 2013;3.
[38] Kosztyán ZT, Katona AI. Risk-based multivariate control chart. Expert Syst Appl 2016;62:250–62.
[39] Kosztyán ZT, Katona AI. Risk-based X-bar chart with variable sample size and sampling interval. Comput Ind Eng 2018;120:308–19.
[40] Katona AI, Saghir A, Hegedűs C, Kosztyán ZT. Design of risk-based univariate control charts with measurement uncertainty. IEEE Access 2023;11:97567–73.
[41] Saghir A, Khan Z, Malela-Majika J-C, Kosztyán ZT. Optimal design of risk-based average charts for autocorrelated measurements. Results Eng 2025;107278.
[42] Wu Z. Asymmetric control limits of the x-bar chart for skewed process distributions. Int J Qual Reliab Manag 1996.
[43] Bennett CA. Effect of measurement error on chemical process control. Ind Qual Control 1954;10(4):17–20.

[44] Kanazuka T. The effect of measurement error on the power of X-R charts. J Qual Technol 1986;18(2):91–5.
[45] Mittag H-J, Stemann D. Gauge imprecision effect on the performance of the XS control chart. J Appl Stat 1998;25(3):307–17.
[46] Linna KW, Woodall WH. Effect of measurement error on shewhart control charts. J Qual Technol 2001;33(2):213–22.
[47] Steiner SH, Cook RJ, Farewell VT, Treasure T. Monitoring surgical performance using risk-adjusted cumulative sum charts. Biostatistics 2000;1(4):441–52.
[48] Knoth S. The art of evaluating monitoring schemes—how to measure the performance of control charts? In: Frontiers in statistical quality control 8. Springer; 2006, p. 74–99.
[49] Saleh NA, Mahmoud MA, Woodall WH. A re-evaluation of repetitive sampling techniques in statistical process monitoring. Qual Technol Quant Manag 2024;21(5):786–804.
[50] Haq A, Woodall WH. A critique on the use of the belief statistic for process monitoring. Qual Reliab Eng Int 2024;40(6):3381–6.
[51] Saleh NA, Mahmoud MA, Keefe MJ, Woodall WH. The difficulty in designing shewhart X and X control charts with estimated parameters. J Qual Technol 2015;47(2):127–38.
[52] Goedhart R, Schoonhoven M, Does RJ. Guaranteed in-control performance for the shewhart X and X control charts. J Qual Technol 2017;49(2):155–71.
[53] Saghir A, Akber Abbasi S, Faraz A. The exact method for designing the maxwell chart with estimated parameter. Comm Statist Simulation Comput 2021;50(1):270–81.
[54] Katona AI. Risk-based statistical process control [Ph.D. thesis], Pannon Egyetem; 2019.
[55] Susilawati A, Atmadio N, Siswanto H. Tool path optimization and cost analysis for manufacturing process of master cylinder piston of motorcycle brake. J Ocean Mech Aerospace-Science Engineering- 2018;55(1):1–5.
[56] Upadhyaya S, Raj D, Gupta K, Saini R, Rana R, Lal R. Designing and analyzing the brake master cylinder for an ATV vehicle. Int J Adv Prod Ind Eng 2020;5(1).
[57] Faraz A, Saniga E, Montgomery D. Percentile-based control chart design with an application to shewhart x and S2 control charts. Qual Reliab Eng Int 2019;35(1):116–26.